RSC Advances

REVIEW

View Article Online
View Journal | View Issue

Cite this: *RSC Adv.*, 2023, **13**, 9065

KuQuinones: a ten years tale of the new pentacyclic quinoid compound

Francesca Valentini, Federica Sabuzi, Mattia Forchetta, Valeria Conte and Pierluca Galloni *

Received 25th January 2023
Accepted 13th March 2023

DOI: 10.1039/d3ra00539a

rsc.li/rsc-advances

Quinones are widespread in nature, as they participate, mainly as redox mediators, in several biochemical processes. Up to now, various synthetic quinones have been recommended in the literature as leading molecules in energy, biomedical and catalytic fields. In this brief review, we retraced our research activity in the last ten years, mainly dedicated to the study of a new class of peculiar pentacyclic conjugated quinoid compounds, synthesized in our group. In particular, their application as sensitive materials in photoelectrochemical devices and in biosensors, as photocatalysts in selective oxidation reactions, and their anticancer activity is here reviewed.

1. Introduction

Since the discovery of coenzyme Q in 1957,[1] several quinone derivatives, playing key roles in nature, have been unveiled. Quinones, thanks to their ability to reversibly accept electrons and protons, take part in numerous natural processes. They are a class of secondary metabolites that can be found in bacteria, fungi, plants and in some animals.[2] Their important role as redox mediators in photosynthesis, in the oxidative phosphorylation and as active antioxidants in the biosynthesis or metabolism of important chemical compounds is well-known.[3]

Quinones are a class of organic compounds composed of at least one six-membered ring, with two ketone groups, respectively in position 1,2 (*o*-quinones) or 1,4 (*p*-quinones), conjugated with two double bonds. Benzoquinone, naphthoquinone and anthraquinone are the most common and investigated scaffolds.

Quinone peculiar features are not limited to their interesting reversible electrochemical behaviour. Indeed, their skeleton can be easily modified[4–7] with the aim to tune their electronic and electrochemical properties, so extending the range of potential applications. Anthraquinones, naphthoquinones and benzoquinones have been used as electroactive compounds in energy storage devices,[8] as redox flow batteries,[9,10] lithium ions batteries,[8] supercapacitors,[11] in water-splitting processes, in hydrogen production, and in n-type Dye Sensitized Solar Cells (n-DSSCs).[12] In addition, quinones possess a privileged scaffold for applications in medicinal chemistry;[7,13] indeed, both synthetic and natural derivatives can act as anticancer,[5,14,15] antibacterial,[16] antifungal, antiviral,[17] anti-Alzheimer and antimalarial[18] drugs. Moreover, they are characterized by interesting antioxidant activity, being also adopted in wound healing treatment.[19] Several synthetic strategies have been developed to synthetize new fluorescent quinone-based probes for bioimaging applications.[20] Anthraquinone derivatives have been employed in photocatalysis to achieve challenging synthetic organic transformations[21] and in sensing applications, to detect anions and metal cations.[22] Therefore, it is evident from the literature the vivid and current interest in quinones chemistry as valid fascinating scaffolds.

Our journey in the quinoid world started more than ten years ago, when a new attractive quinoid compound was unexpectedly obtained by our research group for the first-time.[23] Being its IUPAC name quite intricate, we named it KuQuinone (KuQ) (Fig. 1). In this brief account we summarise our research on KuQuinone chemistry, starting from its challenging synthesis, through its characterization, coming to its applications in photo(electro)chemistry and medicinal chemistry.

2. Synthesis and characterization

Investigation of electron transfer processes occurring in ferrocene-based systems has been one of the main interests of

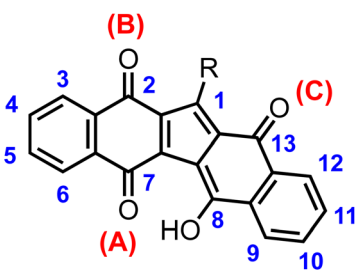

Fig. 1 General structure of KuQuinones, showing numbering of pentacyclic core according to the original paper ref. 23.

Department of Chemical Science and Technologies, University of Rome Tor Vergata, via della ricerca scientifica snc, 00133 Rome, Italy. E-mail: galloni@scienze.uniroma2.it

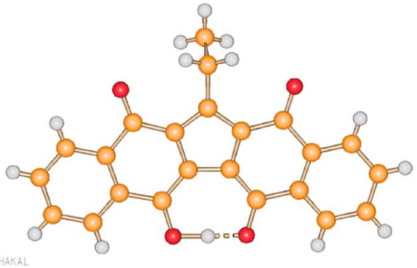

Fig. 2 Molecular structure of compound KuQEt, showing the short intramolecular O–H···O hydrogen bond [O···O 2.499(3) Å]. Reprinted with permission from ref. 23. Copyright 2012 American Chemical Society.

our research group over the past 20 years. In an attempt to synthesize new covalently linked naphthoquinone-ferrocene dyads, an unknown purple compound was unexpectedly obtained.[23] The reaction to obtain the dyad was carried out following the classical protocol for S_N2 reactions, using 2-hydroxy-1,4-naphthoquinone and 11-bromoundecylferrocene as the reagents with K_2CO_3 in dimethyl sulfoxide (DMSO), at 60 °C. However, an unidentified purple powder was obtained as main product. Again, the unknown compound was synthetized using 1-bromobutane and ferrocene in place of 11-bromoundecylferrocene, in the same reaction conditions. X-ray diffraction (Fig. 2) revealed the molecular structure of the unexpected product: a pentacyclic quinoid compound, in which two naphthoquinone molecules were condensed with one molecule of the alkyl bromide, through a five-membered ring. Interestingly, in the molecular structure of the product, there is one less carbon atom than in the reagents. Carbon atom loss presumably occurs from the alkyl bromide, likely *via* the Hooker reaction.[24] Moreover, one carbonyl oxygen was converted to the corresponding enol, that establishes an intra-molecular hydrogen bond with the vicinal carbonyl group, leading to a fully conjugated and planar structure. To note, the reaction mechanism to obtain such an interesting product has not been clarified yet.

A detailed investigation of reaction conditions unveiled that DMSO as solvent, ferrocene as catalyst, bromide as leaving group and an inorganic base were essential for the good outcome of the reaction (Scheme 1).

KuQuinone derivatives bearing different side chains, as alkyl groups, alcohols, esters and phosphonic esters have been obtained over the years, with yields ranging from 6 to 14%, depending on the alkyl bromide (Scheme 1).[23,25–27] Despite not impressive yields, it is important to underline that KuQuinone synthesis is the first reported one-pot reaction to obtain polycyclic quinones. Recently, an alternative procedure for the synthesis of KuQMe has been reported by others.[28] Carboxylic acid KuQ derivatives and phosphonic acids could be obtained through hydrolysis of the corresponding esters in quantitative yields.[25,26]

KuQuinones conjugated and planar structure is responsible of their broad and intense absorption spectrum in the visible region. In particular, the absorption spectra (Fig. 3) are

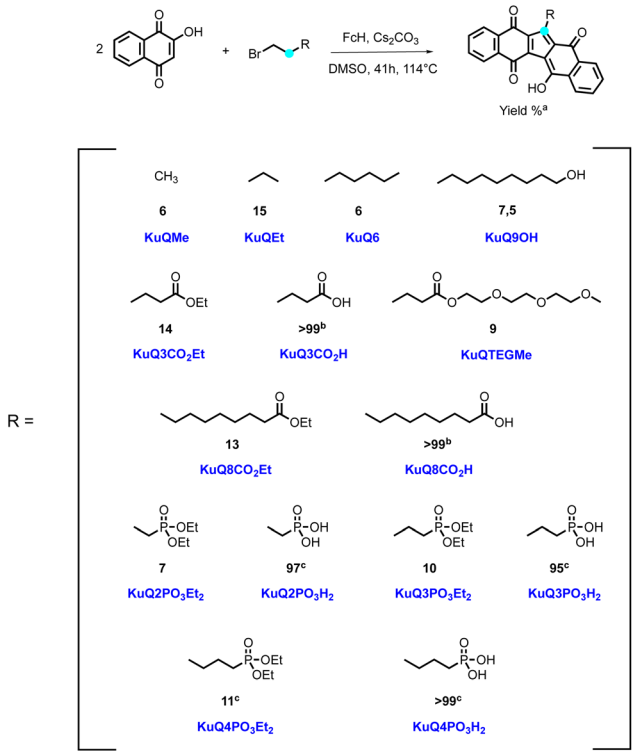

Scheme 1 One-pot synthesis of KuQ derivatives. Reaction conditions: 2-hydroxy-1,4-naphthoquinone 5.75 mmol, alkyl bromide 12 mmol, Cs_2CO_3 8 mmol, ferrocene (FcH) 0.033 mmol, DMSO 22 mL, 41 h, 114 °C.[23,25–27] (a) isolated yield; (b) quantitively obtained through hydrolysis of the corresponding ester. Reaction conditions:[25] KuQ*X*CO_2Et (*X* = 3 or 8) 0.1 mmol in 8 mL THF, NaOH 25% in 2 mL MeOH, 1 h, rt. (c) Quantitively obtained through hydrolysis of the corresponding phosphonate ester. Reaction conditions:[26] KuQ*X*PO_3Et_2 (*X* = 2, 3 or 4) 0.1 mmol, NaI 5 mmol, bromotrimethylsilane 5 mmol, 16 mL dry CH_3CN:$CHCl_3$, 4 h, 40 °C, N_2 atmosphere. Then 30 mL MeOH, 1 h, rt.

characterized by intense bands between 350 and 600 nm. However, significant variation in the shape of the bands and in the molar extinction coefficient can be detected by changing

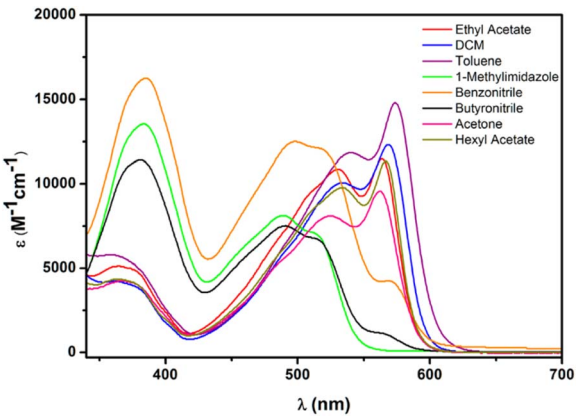

Fig. 3 KuQEt absorption spectra in different solvents. Reprinted with permission from ref. 27. Copyright 2017 American Chemical Society.

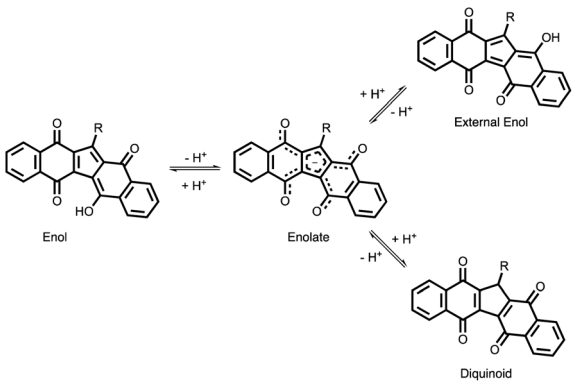

Scheme 2 Possible acid–base equilibrium and keto–enol tautomerization of KuQuinone.

solvent properties. Such differences have been ascribed to the different species of KuQs that can be found in solution.[27]

Considering KuQuinones molecular structure, four different species have been initially supposed to exist in solution, due to acid–base equilibrium and keto–enol tautomerization (Scheme 2):

• The enol form, in which intramolecular hydrogen bond occurs between the enol proton and the vicinal carbonyl oxygen.

• The enolate species, in which enol deprotonation occurs, leading to a negatively charged structure stabilized by resonance.

• The external enol, where intramolecular hydrogen bond is suppressed.

• The diquinoid species, in which conjugation among the 5 rings is interrupted by a sp^3 carbon.

As matter of fact, solvent polarity plays a key role determining which species are prevalent in solution.[27] (Fig. 3) To elucidate KuQ equilibria, a detailed UV-vis and ^{1}H-NMR (Fig. 4) investigation in three different solvents, *i.e.* chloroform, dimethyl sulfoxide and methanol (MeOH), was carried out. KuQ bearing a triethylenglicole side chain (KuQTEGMe) was used in such study, because of its enhanced solubility in polar organic solvents with respect to other derivatives. It is important to underline that functional group variations in side chain does not affect KuQ spectroscopic trait. UV-vis and ^{1}H-NMR data did not support the presence of the external enol and the diquinoid species. Apparently, no keto–enol tautomerization occurs in solution. In addition, DFT calculations pointed out the higher stability of the enol form with respect to the external enol and the diquinoid species. Conversely, KuQ can be found as its enol or enolate species depending on the solvent, thus acid–base equilibrium can be established in solution. Specifically, enol form is exclusively present in apolar and slight polar solvents, such as toluene or $CHCl_3$. Its absorption spectrum is characterized by two intense bands in the visible region centered at 570 nm (ε = 15 000 M^{-1} cm^{-1}) and 531 nm (ε = 13 000 M^{-1} cm^{-1}) and the ^{1}H-NMR spectrum is characterized by a highly deshielded singlet, at 18 ppm, ascribed to the enol proton.[27] (Fig. 4a) On the other hand, enolate is prevalent in polar aprotic solvents, as DMSO (Fig. 4b). The corresponding absorption spectrum shows a general blue shift with respect to the enol, and a diagnostic band at *ca.* 380 nm (λ = 384 nm, ε = 17 000 M^{-1} cm^{-1}; λ = 531 nm, ε = 9000 M^{-1} cm^{-1}; λ = 501 nm, ε = 11 000 M^{-1} cm^{-1}). In MeOH both enol and enolate species were detected. In fact, the absorption spectrum is intermediate between those obtained in chloroform and DMSO. Deprotonation occurring in polar solvents is likely due to the moisture presence. Indeed, pK_a of the enol proton was experimentally and theoretically calculated, through UV-vis and DFT calculations. A pK_a value of 4.7 ± 0.1 was obtained, highlighting the peculiar acidity of such proton.

KuQs acid–base equilibrium also affect their electrochemical behaviour. KuQ enol and enolate were electrochemically characterized through cyclic voltammetry experiments, performed in (CH_2Cl_2)/tetrabutylammonium perchlorate (TBAP) (0.1 M) and *N*,*N*-dimethylformamide DMF/TBAP (0.1 M) solutions, respectively, using KuQEt as model compound.[29] In CH_2Cl_2/TBAP (0.1 M), where the enol form is exclusively present, three quasi-reversible reduction processes were detected ($E_{1/2}^{(1)}$ = −0.30 V, $E_{1/2}^{(2)}$ = −0.87 V, $E_{1/2}^{(3)}$ = −1.26 V *vs.* SCE) (Fig. 5).

Such signals are ascribed to the formation at electrode surface of the monoanion radical, dianion and trianion radical species. Interestingly, the first process results positively shifted

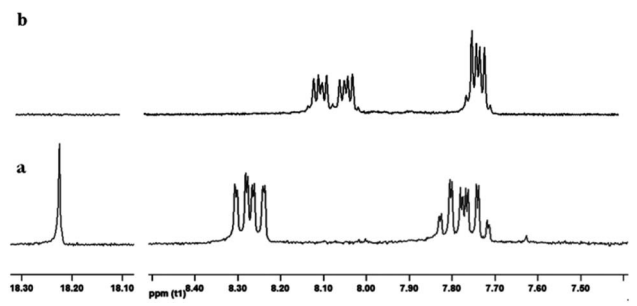

Fig. 4 Comparison between H-NMR spectra of KuQTEGMe in (a) $CDCl_3$, (b) DMSO-d_6. Reprinted with permission from ref. 27. Copyright 2017 American Chemical Society.

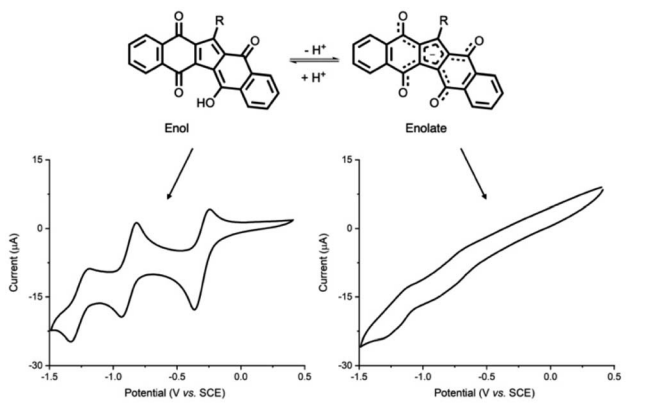

Fig. 5 Cyclic voltammetry of KuQEt in CH_2Cl_2/TBAP 0.1 M (left) and DMF/TBAP 0.1 M (right). WE: glassy carbon, RE: saturated calomel electrode, CE: platinum wire. Adapted from ref. 29. Copyright 2021 The Authors. Published by American Chemical Society.

compared to other biologically important quinones such as vitamin K_1 and bis-coenzyme Q_0.

In a DMF/TBAP (0.1 M) solution, enol deprotonation occurs and KuQuinone enolate, being anionic, show only two broad reduction processes ($E^{(1)}_{1/2} = -0.76$ V, $E^{(2)}_{1/2} = -1.18$ V *vs.* SCE) in which the first peak is negatively shifted (of *ca.* 500 mV) with respect to the same process in CH_2Cl_2 (Fig. 5). Interestingly, KuQ redox chemistry can be tuned, through the introduction of additives in solution, which interact with KuQ carbonyl oxygens, thus promoting reduction processes. Indeed, trifluoroacetic acid (TFA) addition to a KuQEt solution in DMF, led to its protonation, and an excess of the acid favours the three reduction processes, likely because of hydrogen bond between TFA and carbonyl oxygens. Similarly, a positive shift of the reduction processes was observed in CH_2Cl_2 upon the addition of a non-acidic hydrogen bond donor, as 2,2,2-trifluoroethanol (TFE) or a Lewis acid, as scandium triflate (Fig. 6).

DFT calculations suggested the preferred coordination sites for TFE and Sc^{3+} ions. Thanks to these studies, it was possible to speculate that the first and the second reduction processes occur on carbonyl (C) and (B) respectively (Fig. 1). This study was thus instrumental to finely tune the KuQ's redox chemistry in its photo(electro)chemical applications. Furthermore, a spectroscopic characterization of the KuQuinone redox species was carried out through UV-vis-NIR spectroelectrochemistry, also in the presence of Sc^{3+} ions. To note, the absorption spectrum of the monoanion radical species is comparable to the one of the enolate. Upon full reduction of KuQ to $KuQ^{3\bullet-}$, complete re-oxidation to the neutral molecule was allowed only in the presence of Sc^{3+} ions.

3. Photo(electro)chemical applications

The broad and intense absorption spectrum in the visible region and the low first reduction potential make KuQuinones promising dyes and good electron acceptor molecules. For these reasons, they have been employed as photoelectroactive compounds in different photoelectrochemical devices. KuQuinones photoactivity was initially tested anchoring them on indium-tin oxide (ITO) electrodes through Langmuir–Blodgett (LB) technique.[30] Amphiphilic 1-(9-hydroxynonyl)KuQuinone (KuQ9OH) and the less polar 1-methylKuQuinone (KuQMe) were chosen as photosensitizer. Mono and 3-layers of KuQMe and KuQ9OH were efficiently prepared, and the spectroscopic characterization of the modified electrodes revealed the co-existence of the enol and the enolate species on ITO. Upon irradiation, functionalized electrodes produced a stable anodic photocurrent signal in the presence of a sacrificial electron donor species (Fig. 7a) (*i.e.* triethanolamine, TEOA); the resulting action spectra (generated photocurrent *vs.* wavelength) were in good agreement with the absorption spectra of the modified electrodes, demonstrating that KuQ was the photoactive molecule in the cell.

Among the others, the homogenous and well-packed 3-layers film of KuQ9OH on ITO, led to the highest photocurrent value (1.65 μA cm^{-2}) at 530 nm, applying +0.3 V *vs.* Ag/AgCl bias potential (Fig. 7b). This is likely due to the amphiphilic features of the dye, that forms a well-ordered film on the electrode surface. According to the proposed mechanism, upon irradiation KuQ switches to the excited state, becoming a strong oxidant. In this state, it takes an electron from the TEOA in solution, leading to $KuQ^{\bullet-}$, which can give an electron to the conduction band of ITO, closing the circuit and generating anodic photocurrent (Fig. 8). Maximum Incident Photon to Current Efficiency (IPCE%) and internal quantum efficiency (Φ%) for KuQ9OH|ITO electrode were 0.13 and 2.30, respectively. Although these values suffer of the low absorbance of the photoactive material on the electrode, this study unveiled the possibility to use KuQ as photoactive centre in p-type dye sensitized solar cells (p-DSSCs).

Generally, DSSCs are photoelectrochemical devices composed of a semiconductor, a sensitizer, an electrolyte and a counter electrode.[31] Depending on the nature of the semiconductor and on the electron transfer mechanism, n-type DSSCs[32] or p-DSSCs[33] are obtained. p-DSSCs suffer of lower efficiency compared to n-type DSSCs, mostly because of charge

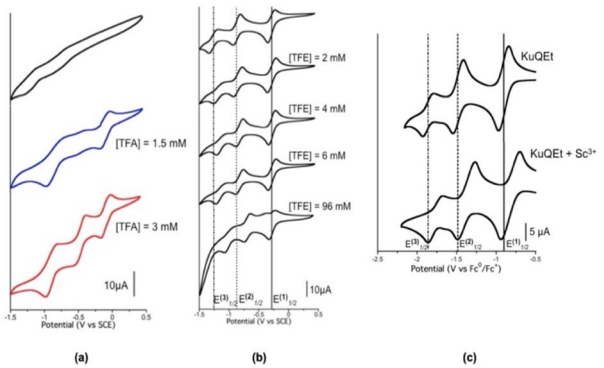

Fig. 6 Cyclic voltammetry of KuQEt in the presence of TFA, TFE, $Sc(OTf)_3$. (a) KuQEt 1 mM DMF/TBAP 0.1 M. (b) KuQEt 2 mM CH_2Cl_2/TBAP 0.1 M. WE: glassy carbon, RE: saturated calomel electrode, CE: platinum wire. (c) KuQEt CH_2Cl_2/TBAP 0.1 M. WE: platinum wire, RE: Ag/Ag^+ electrode, CE: platinum wire. Adapted from ref. 29. Copyright 2021 The Authors. Published by American Chemical Society.

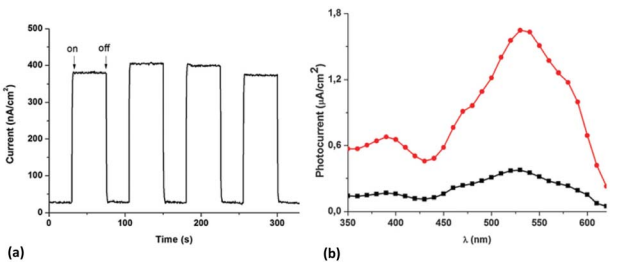

Fig. 7 (a) Photoelectrochemical response of KuQ9OH|ITO upon irradiation at different wavelengths (from 520 nm to 550 nm). (b) Action spectrum of 3-layers KuQ9OH|ITO (red line) and 1-layer KuQ9OH|ITO (black line). Photoelectrochemical conditions: H_2O/Na_2SO_4 0.1 M/TEOA 50 mM, at +0.3 V *vs.* Ag/AgCl. Reproduced from ref. 30 with permission from the Royal Society of Chemistry.

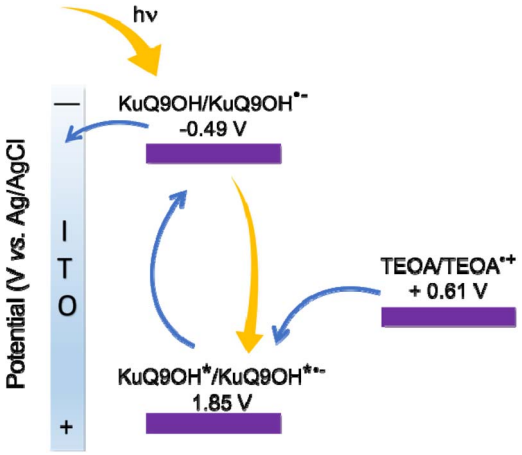

Fig. 8 Proposed mechanism for anodic photocurrent generation of KuQ9OH|ITO/H_2O/Na_2SO_4 0.1 M/TEOA 50 mM.

recombination issues between the dye and the semiconductor, typically NiO.[34] Consequently, great efforts have been made to engineer new dyes, to improve the overall efficiency of p-type cells. Sensitizers used as photoactive components in p-DSSC can be divided into metal complexes[34] and metal free organic dyes.[35–42] Among the latter, push–pull molecules (donor–π–spacer–acceptor),[43–57] and molecular dyads (donor–acceptor)[58–63] gave the best results in terms of generated photocurrent. In the framework of the on-going research of new sensitizers, KuQ have been tested in p-DSSCs.

With such perspective, KuQs bearing a carboxylic acid anchoring group were synthesized to achieve dyes chemisorption on nickel oxide electrodes.[64] Therefore, 1-(3-carboxylpropyl) KuQuinone (KuQ3CO_2H) and 1-(8-carboxyloctyl)KuQuinone (KuQ8CO_2H) were anchored on NiO electrodes.[25] ATR-FTIR characterization confirmed KuQs chemisorption on NiO through the carboxylic group (Fig. 9). KuQ3CO_2H|NiO and KuQ8CO_2H|NiO were tested as photocathodes in p-type DSSC, in the presence of I^-/I_3^- as redox mediator and their performances have been compared with a benchmark sensitizer, as EryB.[42] Results highlighted that KuQ-sensitized cells showed comparable photoelectrochemical efficiency with respect to EryB|NiO. Interestingly, for EryB and other common dyes, the photoinduced charge transfer from the light-absorbing unit to

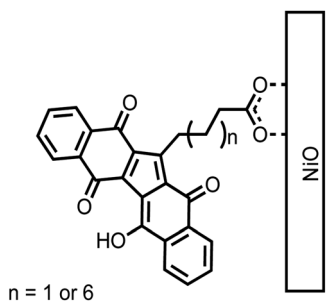

Fig. 9 Schematic representation of KuQ3CO_2H or KuQ8CO_2H chemisorption on NiO.

the electrode occurs through a conjugate π-linker. Conversely, for KuQ-sensitized cells it occurs through the space, being the chain composed of sp^3 carbons. Importantly, this is the first example in which a pentacyclic quinoid core has been employed as photoactive species in a p-DSSC. Although both J_{sc} and η% are lower with respect to the "champions" (push–pull dyes and molecular dyads),[43–46] they are in line with other reported sensitizer,[65] such as diketopyrrolopyrrole,[36,58] carbazole,[66–68] phenoxazine,[37] bodipy,[40] squaraines,[69,70] coumarine[41] and isoindigo[71] derivatives (Fig. 10). These results open the possibility to further modify KuQ molecules, to improve the overall efficiencies.

Later, inspired by such promising results, KuQ3CO_2H was investigated as photosensitizer in dye sensitized photoelectrochemical (DS-PEC) water oxidation devices, using tetraruthenium polyoxomethalate (Ru_4POM) as catalyst and tin oxide (SnO_2) as semiconductor electrode (Fig. 11).[72]

DS-PEC is a promising technology for exploiting solar energy to produce chemical fuels, such as hydrogen, through water splitting reaction.[73] In this device, the photoanode is the electrode where water oxidation to molecular oxygen takes place. To exploit the visible region of the solar spectrum, semiconductor electrodes (as TiO_2, SnO_2, ITO, WO_3) are modified with suitable dyes, and then coupled with a water oxidation catalyst (WOC). Metal-free organic sensitizers are emerging as a new alternative to metal complexes, such as ruthenium(II) polypyridine derivatives.[73] Porphyrins,[74–76] perylenediimide[77–79] derivatives, donor–π–acceptor molecules[80–85] and calixarenes[86] have been exploited with different WOCs, obtaining good to excellent photocurrent and faradaic efficiencies, in terms of oxygen production (Table 1, Fig. 12).

In this field, KuQs may constitute privileged dyes, as they are able to manage proton-coupled electron transfer (PCET), which is a peculiar feature for water oxidation photosynthetic schemes. Moreover, calculated KuQ reduction potential of excited state (*KuQ/KuQ$^{\bullet-}$) stands in the range from +2.12 to +2.16 *vs.* NHE, indicating that KuQ* is a powerful oxidant in PEC water oxidation devices ($E = 0.89$ V *vs.* NHE at pH 5.8 for O_2/H_2O couple). Indeed, KuQ3CO_2H was anchored on SnO_2 and the modified electrode was tested as photoanode using ascorbate as electron donor at pH = 5.8. Photocurrent of 400 μA cm^{-2} at an onset potential of 0.4 V *vs.* NHE was achieved. The mechanism under these conditions is based on KuQ excitation and consequent reductive quenching by ascorbate, with the formation of KuQ$^{\bullet-}$ which is responsible for the electron injection into the conduction band of SnO_2. Coupling of the functionalized electrode with Ru_4POM catalyst generated a constant current of 20 μA cm^{-2} under light irradiation, with an applied potential in the range between 0.4 and 1 V *vs.* NHE. Through a generator-collector method,[72] it was possible to attribute the generated photocurrent to the oxygen evolution. Thus, Ru_4POM|KuQ3CO_2H|SnO_2 achieves water oxidation at low onset potential, with a faradaic efficiency of oxygen evolution of 70 ± 15%, IPCE of 0.09 ± 0.01% and APCE (Absorbed Photon-to-Current Efficiency; IPCE/LHE) of 0.12 ± 0.01% (Fig. 13).

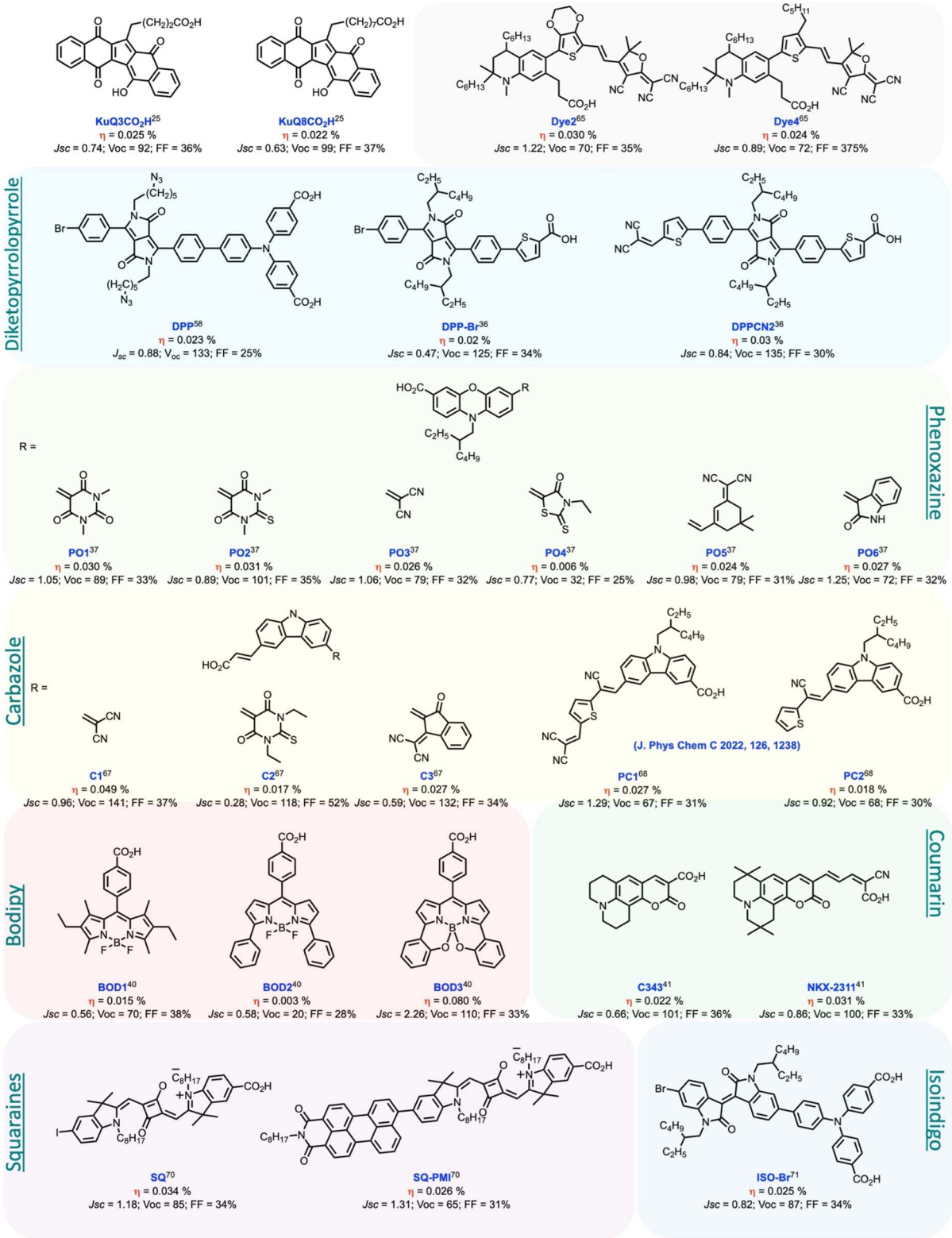

Fig. 10 Comparison of the photoelectrochemical performances between KuQuinones (KuQ3CO2H; KuQ8CO2H) and other photoactive molecules in p-DSSCs (NiO semiconductor, I^-/I_3^- electrolyte). J_{sc} (μA cm^{-2}) = short circuit current density; V_{oc} (mV) = open circuit potential; FF% = Fill Factor; η% = power conversion efficiency.

To improve KuQs efficiency in the photoelectrochemical field and to extend their application on different solid supports, new derivatives bearing a phosphonic acid anchoring unit were synthetized.[26] As a matter of fact, compared to carboxylates, phosphonic acids are better anchoring groups in terms of stability and bond strength on several matrices. However, as in

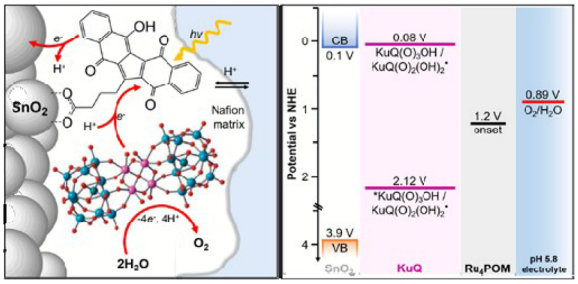

Fig. 11 Schematic representation of $Ru_4POM|KuQ3CO_2H|SnO_2$ photoanodes for water oxidation. The energy levels are shown for the system at pH = 5.8. Reproduced from ref. 72 with permission from the Royal Society of Chemistry.

the case of $KuQ3CO_2H$ and $KuQ8CO_2H$, for the phosphonic acids derivatives the direct synthesis was not achievable. Indeed, using ω-bromoalkylphosphonic acids intramolecular substitution reaction prevalently occurs, thus, diethyl ω-bromoalkylphosphonates reagents had to be firstly synthetized employing α,ω-dibromoalkane and triethyl phosphite (Michaelis–Arbuzov reaction). Such reaction showed several drawbacks, as large excess of dibromoalkane reagents to avoid di-substitution as well as time-consuming purification. An improvement of Michaelis–Arbuzov reaction using an equimolar amount of reagents, to enhance process sustainability, was carried out. With the optimized procedure diethyl ω-bromoalkylphosphonates (ω = 4,5,6) were synthetized with 20–40% yield in 3 hours (Scheme 3). 1-[2-(Diethyl phosphonyl)ethyl] KuQuinone ($KuQ2PO_3Et_2$), 1-[3-(diethyl phosphonyl)propyl] KuQuinone ($KuQ3PO_3Et_2$) and 1-[4-(diethyl phosphonyl)butyl] KuQuinone ($KuQ4PO_3Et_2$) were successfully obtained with 7–11% yields and hydrolysis with bromotrimethylsilane (TMSBr) in the presence of NaI led to the corresponding acids almost quantitively.

Investigation of $KuQ|SnO_2$ electrodes functional parameters was also carried out, to enhance their photoelectrochemical performances.[87] In particular, the effects of tin oxide semiconductor thickness and morphology, the length of the alkyl chain ($KuQ3CO_2H$ *vs.* $KuQ8CO_2H$) and the effect of different anchoring groups ($KuQ3CO_2H$ *vs.* $KuQ3PO_3H_2$) were evaluated in terms of LHE and photocurrent density (*J*) towards the photooxidation of ascorbate. Mesoporous nanostructured SnO_2 films (meso-SnO_2) with different thickness, and vertically oriented SnO_2 nanorods were evaluated toward dye chemisorption. However, the latter could not be tested in photoelectrochemical experiments, being dye chemisorption negligible. The photoelectrochemical response of $KuQ3CO_2H|$meso-SnO_2 electrodes was tested in the presence of aqueous ascorbate buffer, pH = 5.8 (Fig. 14). Although, high thickness led to an increase in LHE, an abatement of 50% in photocurrent density was observed using 5 μm film, likely due to charge recombination issues. Thus, meso-SnO_2 with 2.5 μm film thickness was chosen as model electrode. $KuQ8CO_2H|$meso-SnO_2 and $KuQ3PO_3H_2|$meso-SnO_2 performances were then evaluated. Although, dye loading was similar, the photocurrent density drastically decreased with $KuQ8CO_2H$ photosensitizer, likely because of the long distance of the light absorbing unit from the electrode (8 sp^3 carbons); therefore, electron transfer efficiency was reduced with respect to $KuQ3CO_2H$. Moreover, $KuQ3PO_3H_2|$meso-SnO_2 showed significantly lower LHE with respect to $KuQ3CO_2H|$meso-SnO_2 (55% *vs.* 93%) and consequently a reduction of photocurrent density (200 μA cm^{-2} *vs.* 350 μA cm^{-2} at 0.1 V *vs.* Ag/AgCl). Thus, carboxylic acid anchoring group maintained the best performances on SnO_2 electrodes.

To elucidate the mechanism of electron injection from the dye to the semiconductor, an *ab initio* modelling of the $KuQ3CO_2H|$meso-SnO_2 was carried out. Results supported the previously proposed mechanistic pathway, in which reductive

Table 1 Selected examples of DS-PEC photoanode for water oxidation reaction

Photoanode[a]	Photocurrent density (μA cm^{-2})	Faradaic efficiency (%)	IPCE (%)	Bias	pH	Light source (mW cm^{-2})	References
$TiO_2|KuQ3CO_2H|Ru_4POM$	20	70	0.09	0.4 V *vs.* NHE	5.8	100	72
$ITO|PMPDI|CoO_x$	150	80	0.12	1.0 V *vs.* Ag/AgCl	7	100	77
$TiO_2|L0|Ru(pdc)^b(pic)^c{}_3$	300	73	25[d]	0 V *vs.* Ag/AgCl	7	100	80
$SnO_2|PMPDI|CoO_x$	50	31	n.r.	0.9 *vs.* Ag/AgCl	7	100	78
$SnO_2|P|IrCp^e$	8	80	0.9	0.8 V *vs.* NHE	6	100	74
$TiO_2|BDPy|Ru(bda)^f(pic)^c(pmp)^g$	*Ca.* 60	76	4	0.2 V *vs.* NHE	7.2	200	99
$TiO_2|CBZ\text{-}Th|Ru(bda)^f(pic)^c{}_2$	37	69	n.r.	0.2 V *vs.* Ag/AgCl	6.5	70	83
$SnO_2/TiO_2|Org1|ALD^h\text{-}Al_2O_3|RuP^{2+}\text{-}Ru(bda)(L)^i{}_2$	500	97	*Ca.* 14	0.4 V *vs.* Ag/AgCl	4.65	100	81
$nanoWO_3|PBI_5Ru_4POM$	*Ca.* 7	97	0.50	0.9 V *vs.* RHE	3	100	79
$TiO_2|[CoFe\text{-}JG]$	*Ca.* 50	83	n.r.	1.23 V *vs.* RHE	7	100	85
$TiCl_4\text{-}mesoTiO_2|DPP\text{-}RuWOC$ (dyad)	17	44	n.r.	0.2 V *vs.* NHE	5.6	100	100
$TiO_2|C4BTP\text{-}Ru(bda)^f(4,4'\text{-}bpy)^j$	42	46	n.r.	0 V	n.s.	300 W	86
$TiO_2|CBZ\text{-}3Py$ + RuWOC (dyad)	25	88	16	0.5 V *vs.* NHE	5.8	200 W	84
$TiO_2|TPA|PNO^k|Ru(bda)^f$(4-hexylpyridine)	520	82	30	0.4 V *vs.* NHE	7	100	82

[a] The structures of the dyes are reported in Fig. 12. [b] pdc = pyridine-2,6-dycaboxylic acid. [c] pic = 4-picoline. [d] IPCE was measured for tandem-DSPEC. [e] Cp = pentamethylcyclopentadienyl. [f] bda = 2,2′-bipyridine-6,6′-dicarboxylate. [g] pmp = (4-pyridil)methylphosphonic acid. [h] ALD = atomic layer deposition. [i] L = 4-PyridilO$(CH_2)_3PO_3H_2$. [j] 4,4′-bpy = 4,4′-bipyridine. [k] PNO = 4-hexylpyridine *N*-oxide; n.r. = not reported by the authors; n.s. = not specified by the authors.

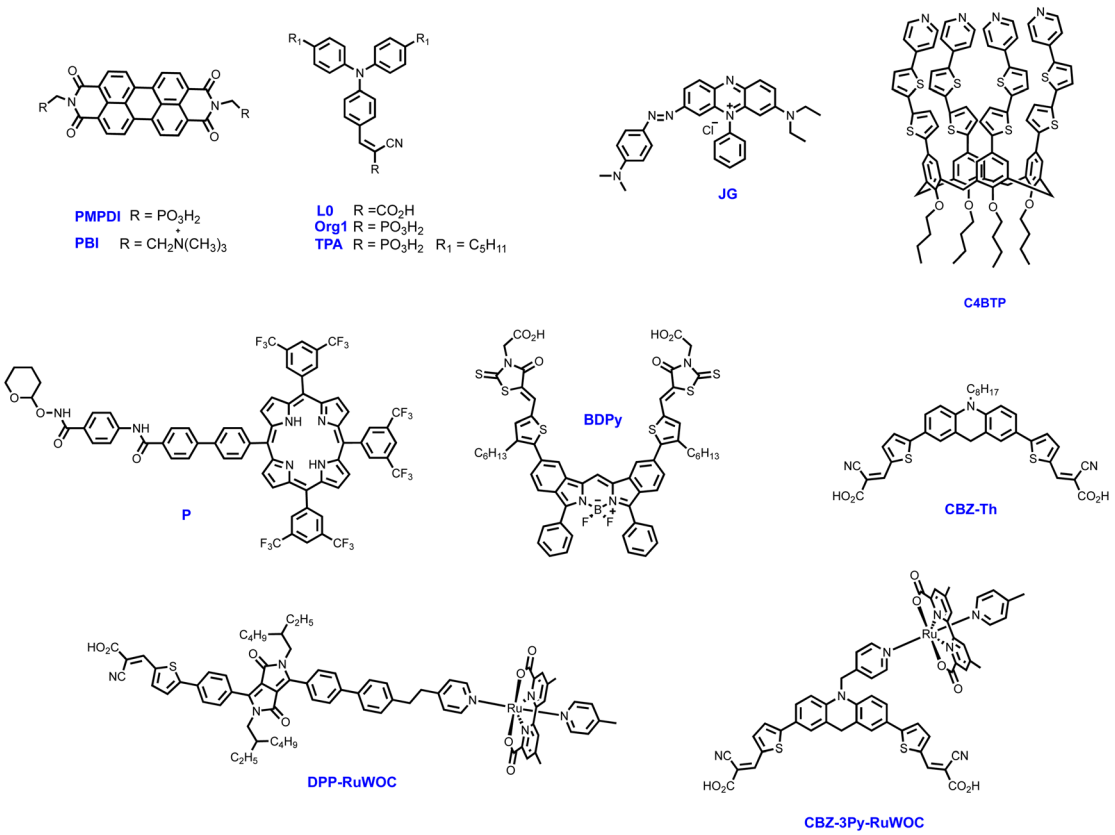

Fig. 12 Molecular structures of the dyes reported in Table 1.

quenching of the KuQ excited species (KuQ*) likely occurred trough a PCET mechanism.

KuQ3CO_2H|meso-SnO_2 photoanode was also tested in the PEC oxidation of benzyl alcohol, both in aqueous and organic medium. The most interesting results were obtained in acetonitrile, using pyridine as base and *N*-hydroxysuccinimide as redox mediator. Preliminary data demonstrated that KuQs are promising dyes for the photoelectrochemical oxidation of alcohols.

In recent years, photoelectrochemical (PEC) sensing has emerged as new analytical method because of its high signal-to-noise ratio and sensitivity.[88] However, within dye sensitized PEC sensors, only few papers have been reported,[89–92] and the number is even less when considering a metal-free dye sensitized PEC sensor.[93–97] In the framework of photoelectrochemical applications, recently KuQ3CO_2H has been employed as dye in the first photoelectrochemical (bio)sensor for ethanol detection (Fig. 15).[98] The biosensor was composed of a screen-printed electrode (SPE), which constitutes a cost-effective and miniaturized electrochemical cell, modified by a layer of carbon black (CB) dispersion. A nanocomposite composed of KuQ3CO_2H anchored on TiO_2 was casted on CB layer. Photoelectrochemical biosensors modification with KuQ is strategic because it allows the use of visible light instead of UV irradiation. SPE-CB-KuQ3CO_2H/TiO_2 proved to be a reliable sensor for NADH detection, showing linear correlation between NADH concentration and generated photocurrent, in the range between 50 μM and 8 mM, with a detection limit of 20 μM, using Tris buffer at pH 8.8 as working solution and 0.4 V applied potential *vs.* Ag pseudoreference. The biosensor was then modified with alcohol dehydrogenase enzyme and its NAD^+ cofactor. The aim was to detect ethanol in solution, exploiting the enzymatic reaction:

$$\text{Ethanol} + \text{NAD}^+ \rightleftarrows \text{acetaldehyde} + \text{NADH} + \text{H}^+$$

Again, a linear correlation between ethanol concentration and generated photocurrent was achieved, demonstrating that CB-KuQ3CO_2H/TiO_2 is able to regenerate the coenzyme NAD^+ even in the immobilized form. Finally, to demonstrate its applicability, the biosensor was employed to detect ethanol in a real sample of white wine, obtaining reliable results with a good recovery value of 91.60 ± 0.01%. Noteworthy, the analytical performances of such new photoelectrochemical biosensor open the way for realizing other biosensors combined with different Dehydrogenase enzymes, so extending the applicability of such devices.

4. Photochemical applications

It has been largely reported that KuQuinone in its excited state is a strong oxidant.[25,30,72,87] Considering its broad and intense absorption spectrum in the visible region, 1-hexylKuQuinone (KuQ6) has been recently employed for the first time as a homogenous organophotocatalyst for the selective oxidation

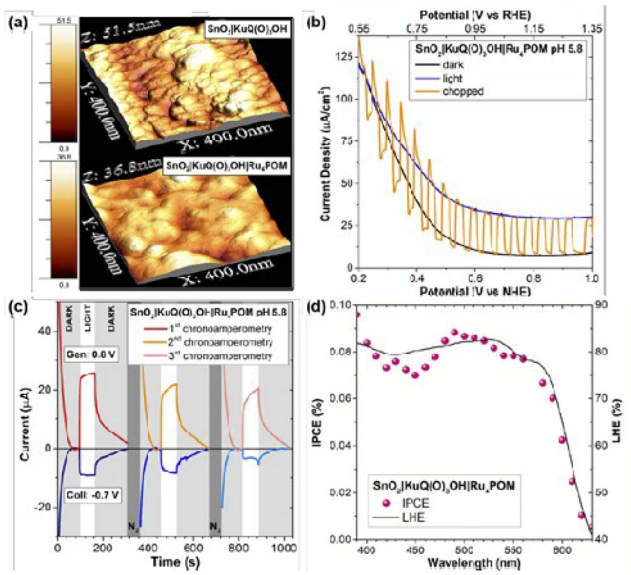

Fig. 13 (a) AFM images of KuQ3CO$_2$H|SnO$_2$ and Ru$_4$-POM|KuQ3CO$_2$H|SnO$_2$ photoanodes. (b) Linear sweep voltammetry for Ru$_4$POM|KuQ3CO$_2$H|SnO$_2$ (CE: Pt; RE: Ag/AgCl 3 M NaCl; 20 mV s^{-1}; light: AM 1.5G + 400 nm cut-off filter). (c) Consecutive G-C experiments for O_2 detection with Ru$_4$POM|KuQ3CO$_2$H|SnO$_2$; the positive photocurrent (red, orange, pink traces) is accompanied by a negative current of O_2 reduction at the FTO collector (blue, light blue, azure traces); CE: Pt; RE: Ag/AgCl 3 M NaCl; light: white LED + 400 nm cut-off filter. (d) IPCE (purple dots) and LHE (black line) of Ru$_4$POM|KuQ3CO$_2$H|SnO$_2$. Water oxidation conditions: 0.1 M Na_2SiF_6/$NaHCO_3$ buffer at pH 5.8. Reproduced from ref. 72 with permission from the Royal Society of Chemistry.

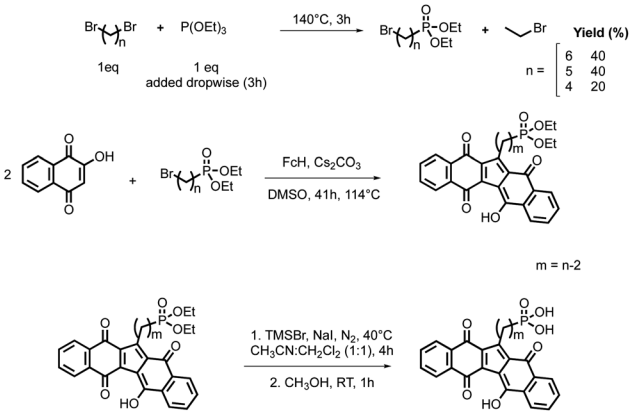

Scheme 3 Stepwise synthesis of KuQXPO$_3$Et$_2$ (X = 2, 3, 4).

of thioethers to sulfoxides, using O_2 as oxidant.[101] The reaction was initially explored using thioanisole as model substrate (Scheme 4). Remarkably, full substrate conversion to methyl phenyl sulfoxide was achieved with 0.5% KuQ in just 90 minutes irradiation with a green LED (30 W, λ = 520 nm) in 1,1,1,3,3,3-hexafluoro-2-propanol (HFIP) and O_2 atmosphere. No over-oxidation product was detected. Quantitative oxidation was obtained also in air atmosphere (1% KuQ, 90 min) and on a gram-scale (0.5% KuQ, 20 h). Recently, several homogenous

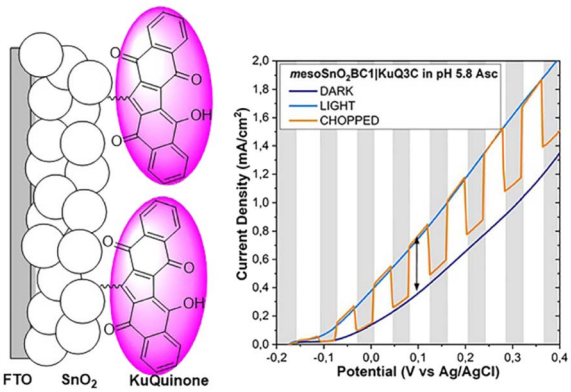

Fig. 14 LSV of KuQ3CO$_2$H|meso-SnO$_2$ in aqueous ascorbate buffer pH 5.8, 20 mV s^{-1}, light: AM 1.5G + 400 nm cut-off filter. Reproduced from ref. 87.

photocatalysts have been used in thioethers oxidation,[102] as flavin derivatives,[103] bodipy[104,105] and thioxanthone[106,107] derivatives, showing high yields and from good to excellent selectivity to sulfoxides. However, recyclability of the homogenous system in such reactions is an understudied field. Remarkably, rechargeability and recyclability studies demonstrated the great robustness of KuQ, that could be used for at least 20 runs, leading to almost quantitative thioanisole oxidation and reaching TONs higher than 4000. Furthermore, a wide substrate scope is tolerated: 17 substrates, including differently p-substituted thioanisole derivatives, also bearing easily oxidable functional groups, diaryl, dibenzyl, aliphatic and cyclic thioethers were efficiently oxidized to the corresponding sulfoxides in less than 2 h. Moreover, KuQ is also able to oxidize aromatic organosulfur compounds, as dibenzothiophene and 4,6-dimethyldibenzothiophene, whose oxidation is interesting in the field of fuel desulfurization. In addition, the mono-oxidation of thianthrene-5-oxide, an efficient reagent for valuable organic transformations, was achieved in 4.5 h with 5% KuQ. The reaction mechanism involves KuQ excitation to KuQ*, that can oxidize thioether ($PhSCH_3$) to the radical cation species ($PhSCH_3^{\bullet+}$), forming $KuQ^{\bullet-}$. $PhSCH_3^{\bullet+}$ interacts with one molecule of molecular dioxygen, leading to $PhS(CH_3)$-$OO^{\bullet+}$. The latter reacts with an additional molecule of sulfide, forming $[PhS(CH_3)–O–O–S(CH_3)Ph]^{\bullet+}$ intermediate, which evolves to the formation of two molecules of the sulfoxide, through an electron transfer by $KuQ^{\bullet-}$, restoring the photocatalyst, or by an additional molecule of the substrate, which is then converted to the radical cation, thus continuing the cycle (Scheme 5).

Therefore, KuQ can be considered as a new emerging robust metal-free photocatalyst to be further explored in sustainable oxidation reactions.

5. Anticancer activity

Inspired by the structural similarity of KuQs with Camptothecin and Topotecan, widely used anticancer agents having a pentacyclic core, and considering the interesting bioactivity of several synthetic and natural quinones,[5,14,17] we investigated KuQ

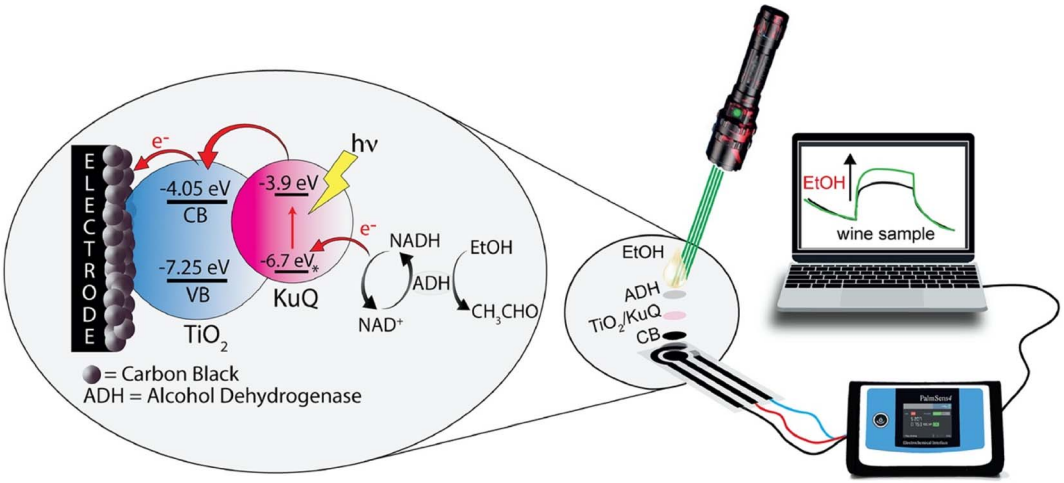

Fig. 15 Scheme of the photoelectrochemical sensing system and the experimental set-up for detection of ethanol. Reprinted from ref. 98. Copyright 2022, with permission from Elsevier.

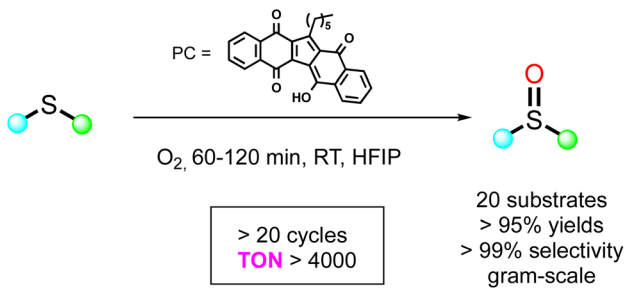

Scheme 4 Photocatalytic thioethers oxidation.

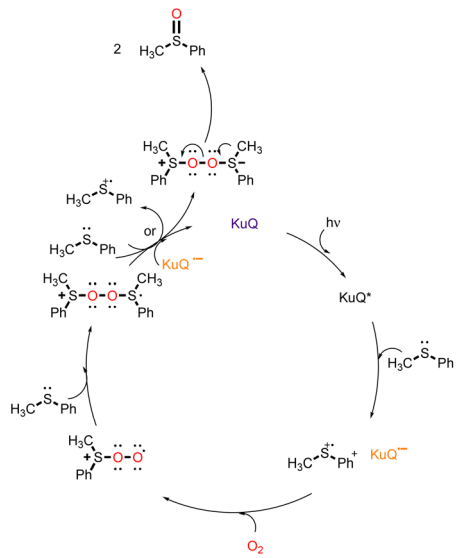

Scheme 5 Proposed mechanism for thioether photooxidation promoted by KuQ.

cytotoxic activity against model human cancer cells. Therefore, cell lines SKOV3 and SW480, established for ovarian and colon pathologies, respectively, have been screened.[23] Cisplatin was used as control, and results revealed that the KuQEt capability to inhibit cells growth was comparable or even higher than that of cisplatin. In addition, negligible cytotoxicity against human fibroblast was observed. To elucidate the mechanism of action, KuQEt activity as DNA topoisomerases (Top) inhibitor was studied,[108] in analogy with the mechanism of Camptothecin and Topotecan.[14] In fact, topoisomerases are well-characterized molecular targets for cancer therapy. CPT is the traditional Top inhibitors; however, it showed important dose-limiting toxicities and drug resistance. Thus, the research of new anti-cancer drugs acting as Top inhibitors is in great demand. Results indicated that KuQEt acts as inhibitor of the oligonucleotide cleavage and its interaction with the enzyme is reversible. Remarkably, it was the first time that a small organic compound showed the ability to stimulate Top I religation reaction, even in the presence of the cleavage inhibitor CPT. Molecular docking experiments highlighted KuQEt structural features, likely responsible for the cleavage inhibition and religation effect (Fig. 16).

Afterwards, several KuQ derivatives, namely, KuQMe, KuQEt, KuQ6, KuQ9OH, KuQ3CO$_2$Et, KuQ3CO$_2$H, KuQTEG, were

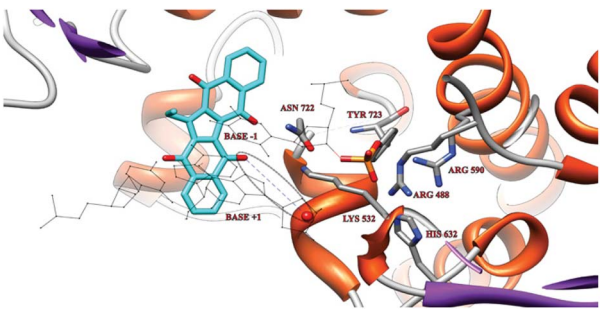

Fig. 16 Representative structure of KuQEt docked on the covalent Top1 + DNA binary complex. It is highlighted with a grey oval the interaction between 5′ DNA end (red sphere) and the closest KuQEt oxygen acceptor. Reproduced from ref. 108.

evaluated as inhibitors of the growth of SKOV3 and SW480 cell lines by the colorimetric MTT assay.[27] Regarding SW480 cell lines results clearly showed that the nature of KuQ side chain influenced the cellular uptake rather than trigger the drug resistance mechanism. Indeed, KuQTEG showed the lowest IC_{50} value (1.5 ± 2 μM) and Ku9OH the highest one (21.5 ± 2 μM). Conversely, for SKOV3 cell line, a wide variation of IC_{50} was observed (from 5 μM to 52 μM), thus suggesting a different cellular membrane composition between the two cell lines. Overall, KuQ6 showed the best results in terms of IC_{50} for both cancer cell lines as well as for healthy human fibroblast, indicating high specific activity toward tumor cell. These studies highlighted the promising use as anticancer drug of KuQ.

6. Conclusions

In this brief review, we have looked back to the research activity of our group in the last ten years, which has been mostly focused on the study of a new class of organic compounds, called KuQuinones. Although, they were firstly synthesized by serendipity, the profound investigation of their structural, electronic and electrochemical features allowed to unveil the numerous applications of KuQuinones. Indeed, the outstanding properties of this novel compounds deserved to be exploited in several interesting applications and they resulted strategical for KuQ usage in different fields, as in photoelectrochemistry, in photocatalysis, as well as in medicinal chemistry.

Due to their fascinating features, further potential applications of KuQuinones are still under investigation, with the aim to offer new possibilities in catalysis, energy, sensors and in medical fields.

Conflicts of interest

The authors declare no conflict of interest.

References

1 F. L. Crane, Y. Hatefi, R. L. Lester and C. Widmer, *Biochim. Biophys. Acta*, 1957, **25**, 220–221.
2 R. H. Thomson, *Naturally occurring quinones IV—Recent advances*, Springer, Dordrecht, Berlin, 1997.
3 M. Liu and S. Lu, *Front. Plant Sci.*, 2016, **7**, 1898–1916.
4 A. S. de Souza, R. C. B. Ribeiro, D. C. S. Costa, F. P. Pauli, D. R. Pinho, M. G. de Moraes, F. de C. da Silva, L. da S. M. Forezi and V. F. Ferreira, *Beilstein J. Org. Chem.*, 2022, **18**, 381–419.
5 J. C. Boulos, M. Rahama, M. F. Hegazy and T. Efferth, *Cancer Lett.*, 2019, **459**, 248–267.
6 M. S. Malik, R. I. Alsantali, R. S. Jassas, A. A. Alsimaree, R. Syed, M. A. Alsharif, K. Kalpana, M. Morad, I. I. Althagafia and S. A. Ahmed, *RSC Adv.*, 2021, **11**, 35806–35827.
7 M. Devi, P. Kumar, R. Singh, L. Narayan, A. Kumar, J. Sindhu, S. Lal, K. Hussain and D. Singh, *J. Mol. Struct.*, 2022, **1269**, 133786–133825.
8 C. Han, H. Li, R. Shi, T. Zhang, J. Tong, J. Lia and B. Li, *J. Mater. Chem. A*, 2019, **7**, 23378–23415.
9 P. Symons, *Curr. Opin. Electrochem.*, 2021, **29**, 100759–100765.
10 D. G. Kwabi, Y. Ji and M. J. Aziz, *Chem. Rev.*, 2020, **120**, 6467–6489.
11 S. P. Ega and P. Srinivasan, *J. Energy Storage*, 2022, **47**, 103700–103727.
12 E. J. Son, J. H. Kim, K. Kima and C. B. Park, *J. Mater. Chem. A*, 2016, **4**, 11179–11202.
13 L. Zhang, G. Zhang, S. Xu and Y. Song, *Eur. J. Med. Chem.*, 2021, **223**, 113632–113647.
14 X. Liang, Q. Wu, S. Luan, Z. Yin, C. He, L. Yin, Y. Zou, Z. Yuan, L. Li, X. Song, M. He, C. Lv and W. Zhang, *Eur. J. Med. Chem.*, 2019, **171**, 129–168.
15 M. S. Malik, R. I. Alsantali, R. S. Jassas, A. A. Alsimaree, R. Syed, M. A. Alsharif, K. Kalpana, M. Morad, I. I. Althagafia and S. A. Ahmed, *RSC Adv.*, 2021, **11**, 35806–35827.
16 J. Daia, R. Hand, Y. Xud, N. Lie, J. Wanga and W. Danc, *Bioorg. Chem.*, 2020, **101**, 103922–103947.
17 E. N. da Silva Júnior, G. A. M. Jardim, C. Jacob, U. Dhawa, L. Ackermann and S. L. de Castro, *Eur. J. Med. Chem.*, 2019, **179**, 863–915.
18 O. P. S. Patel, R. M. Beteck and L. J. Legoabe, *Eur. J. Med. Chem.*, 2021, **210**, 113084–113111.
19 O. Yazarlu, M. Iranshahi, H. R. K. Kashani, S. Reshadat, S. Habtemariam, M. Iranshahy and M. Hasanpour, *Pharmacol. Res.*, 2021, **174**, 105841–105878.
20 G. G. Dias, A. King, F. de Moliner, M. Vendrell and E. N. da Silva Júnior, *Chem. Soc. Rev.*, 2018, **47**, 12–27.
21 J. Cervantes-González, D. A. Vosburg, S. Mora-Rodriguez, M. A. Vázquez, L. G. Zepeda, C. V. Gómeza and S. Lagunas-Riverad, *ChemCatChem*, 2020, **12**, 3811–3827.
22 G. Navneet Kaur, *Inorg. Chim. Acta*, 2022, **536**, 120917–120943.
23 A. Coletti, S. Lentini, V. Conte, B. Floris, O. Bortolini, F. Sforza, F. Grepioni and P. Galloni, *J. Org. Chem.*, 2012, **77**, 6873–6879.
24 K. Lee, P. Turnbull and H. W. Moore, *J. Org. Chem.*, 1995, **60**, 461–464.
25 M. Bonomo, F. Sabuzi, A. Di Carlo, V. Conte, D. Dini and P. Galloni, *New J. Chem.*, 2017, **41**, 2769–2779.
26 M. Forchetta, V. Conte, G. Fiorani, P. Galloni and F. Sabuzi, *Organics*, 2021, **2**, 107–117.
27 F. Sabuzi, S. Lentini, F. Sforza, S. Pezzola, S. Fratelli, O. Bortolini, B. Floris, V. Conte and P. Galloni, *J. Org. Chem.*, 2017, **82**, 10129–10138.
28 M. Onuki, M. Ota, S. Otokozawa, S. Kamo, S. Tomoshige, K. Tsubaki and K. Kuramochi, *Tetrahedron*, 2020, **76**, 130899–130908.
29 F. Valentini, F. Sabuzi, V. Conte, V. N. Nemykin and P. Galloni, *J. Org. Chem.*, 2021, **86**, 5680–5689.
30 F. Sabuzi, V. Armuzza, V. Conte, B. Floris, M. Venanzi, P. Galloni and E. Gatto, *J. Mater. Chem. C*, 2016, **4**, 622–630.
31 A. Mishra, M. K. R. Fischer and P. Bäuerle, *Angew. Chem., Int. Ed.*, 2009, **48**, 2474–2499.

32 A. Hagfeldt, G. Boschloo, L. Sun, L. Kloo and H. Pettersson, *Chem. Rev.*, 2010, **110**, 6595–6662.
33 F. Odobel, L. Le Pleux, Y. Pellegrin and E. Blart, *Acc. Chem. Res.*, 2010, **43**, 1063–1071.
34 E. Benazzi, J. Mallows, G. H. Summers, F. A. Black and E. A. Gibson, *J. Mater. Chem. C*, 2019, **7**, 10409–10445.
35 J. He, H. Lindström, A. Hagfeldt and S. Lindquist, *J. Phys. Chem. B*, 1999, **103**, 8940–8943.
36 L. Favereau, J. Warnan, Y. Pellegrin, E. Blart, M. Boujtita, D. Jacquemin and F. Odobel, *Chem. Commun.*, 2013, **49**, 8018–8020.
37 K. S. Keremane, A. Planchat, Y. Pellegrin, D. Jacquemin, F. Odobel and A. Vasudeva Adhikari, *ChemSusChem*, 2022, **15**, e202200520.
38 O. Langmar, D. Saccone, A. Amat, S. Fantacci, G. Viscardi, C. Barolo, R. D. Costa and D. M. Guldi, *ChemSusChem*, 2017, **10**, 2385–2393.
39 Y. Farré, F. Maschietto, J. Föhlinger, M. Wykes, A. Planchat, Y. Pellegrin, E. Blart, I. Ciofini, L. Hammarström and F. Odobel, *ChemSusChem*, 2020, **13**, 1844–1855.
40 N. T. Z. Potts, T. Sloboda, M. Wächtler, R. Agung Wahyuono, V. D'Annibale, B. Dietzek, U. B. Cappel and E. A. Gibson, *J. Chem. Phys.*, 2020, **153**, 184704.
41 S. Mori, S. Fukuda, S. Sumikura, Y. Takeda, Y. Tamaki, E. Suzuki and T. Abe, *J. Phys. Chem. C*, 2008, **112**, 16134–16139.
42 J. He, H. Lindström, A. Hagfeldt and S. Lindquist, *Sol. Energy Mater. Sol. Cells*, 2000, **62**, 265–273.
43 I. R. Perera, T. Daeneke, S. Makuta, Z. Yu, Y. Tachibana, A. Mishra, P. Bäuerle, C. A. Ohlin, U. Bach and L. Spiccia, *Angew. Chem., Int. Ed.*, 2015, **54**, 3758–3762.
44 Q. Zhang, K. Jiang, J. Huang, C. Zhao, L. Zhang, X. Cui, M. Su, L. Yang, Y. Song and X. Zhou, *J. Mater. Chem. A*, 2015, **3**, 7695–7698.
45 C. J. Wood, G. H. Summers and E. A. Gibson, *Chem. Commun.*, 2015, **51**, 3915–3918.
46 Y. Farré, M. Raissi, A. Fihey, Y. Pellegrin, E. Blart, D. Jacquemin and F. Odobel, *ChemSusChem*, 2017, **10**, 2618–2625.
47 Z. Liu, D. Xiong, X. Xu, Q. Arooj, H. Wang, L. Yin, W. Li, H. Wu, Z. Zhao, W. Chen, M. Wang, F. Wang, Y. Cheng and H. He, *ACS Appl. Mater. Interfaces*, 2014, **6**, 3448–3454.
48 Z. Liu, W. Li, S. Topa, X. Xu, X. Zeng, Z. Zhao, M. Wang, W. Chen, F. Wang, Y. Cheng and H. He, *ACS Appl. Mater. Interfaces*, 2014, **6**, 10614–10622.
49 H. Ye, L. Shen, S. Zhang, X. Li, F. Yu, R. Diao and J. Hua, *ACS Omega*, 2018, **3**, 14448–14456.
50 B. Jin, W. Wu, X. Zhang, F. Guo, Q. Zhang and J. Hua, *Chem. Lett.*, 2013, **42**, 1271–1272.
51 F. Wu, L. Zhu, S. Zhao, Q. Song and C. Yang, *Dyes Pigm.*, 2016, **124**, 93–100.
52 Y. Farré, M. Raissi, A. Fihey, Y. Pellegrin, E. Blart, D. Jacquemin and F. Odobel, *Dyes Pigm.*, 2018, **148**, 154–166.
53 P. Qin, H. Zhu, T. Edvinsson, G. Boschloo, A. Hagfeldt and L. Sun, *J. Am. Chem. Soc.*, 2008, **130**, 8570–8571.
54 J. Cui, J. Lu, X. Xu, K. Cao, Z. Wang, G. Alemu, H. Yuang, Y. Shen, J. Xu, Y. Cheng and M. Wang, *J. Phys. Chem. C*, 2014, **118**, 16433–16440.
55 K. A. Click, D. R. Beauchamp, B. R. Garrett, Z. Huang, C. M. Hadad and Y. Wu, *Phys. Chem. Chem. Phys.*, 2014, **16**, 26103–26111.
56 G. H. Summers, J. Lefebvre, F. A. Black, E. S. Davies, E. A. Gibson, T. Pullerits, C. J. Wood and K. Zidek, *Phys. Chem. Chem. Phys.*, 2016, **18**, 1059–1070.
57 R. Brisse, C. Praveen, V. Maffeis, T. Bourgeteau, D. Tondelier, T. Berthelot, B. Geffroy, T. Gustavsson, J. M. Raimundo and B. Jousselme, *Sustainable Energy Fuels*, 2018, **2**, 648–654.
58 Y. Bentounsi, K. Seintis, S. Diring, E. Vauthey and F. Odobel, *ACS Appl. Energy Mater.*, 2021, **4**, 2629–2636.
59 Y. Higashino, S. Erten-Elab and Y. Kuboa, *Dyes Pigm.*, 2019, **170**, 107613–107621.
60 M. Bonomo, A. Carella, F. Borbone, L. Rosato, D. Dini and L. Gontrani, *Dyes Pigm.*, 2020, **175**, 108140–108153.
61 A. Reddy Marri, H. Flint, E. A. Gibson and J. Fielden, *Dyes Pigm.*, 2022, **202**, 110244–110252.
62 L. Le Pleux, A. L. Smeigh, E. Gibson, Y. Pellegrin, E. Blart, G. Boschloo, A. Hagfeldt, L. Hammarström and F. Odobel, *Energy Environ. Sci.*, 2011, **4**, 2075–2084.
63 M. Bonomo, A. Di Carlo, R. Centore, D. Dini and A. Carella, *Sol. Energy*, 2018, **169**, 237–241.
64 Y. Pellegrina, L. Le Pleuxa, E. Blart, A. Renauda, B. Chavillon, N. Szuwarskia, M. Boujtitaa, L. Cario, S. Jobic, D. Jacquemin and F. Odobel, *J. Photochem. Photobiol., A*, 2011, **219**, 235–242.
65 Y. Hao, C. J. Wood, C. A. Clark, J. A. Calladine, R. Horvath, M. W. D. Hanson-Heine, X. Sun, I. P. Clark, M. Towrie, M. W. George, X. Yang, L. Sun and E. A. Gibson, *Dalton Trans.*, 2016, **45**, 7708–7719.
66 L. Bao, P. Ho, R. Kumar Chitumalla, J. Jang, S. Thogiti and J. Kim, *Dyes Pigm.*, 2018, **149**, 25–36.
67 A. Carella, R. Centore, F. Borbone, M. Toscanesi, M. Trifuoggi, F. Bella, C. Gerbaldi, S. Galliano, E. Schiavo, A. Massaro, A. B. Muñoz-García and M. Pavone, *Electrochim. Acta*, 2018, **292**, 805–816.
68 K. S. Keremane, Y. Pellegrin, A. Planchat, D. Jacquemin, F. Odobel and A. Vasudeva Adhikari, *J. Phys. Chem. C*, 2022, **126**, 12383–12390.
69 M. Bonomo, D. Saccone, C. Magistris, A. Di Carlo, C. Barolo and D. Dini, *ChemElectroChem*, 2017, **4**, 2385–2397.
70 J. Warnan, J. Gardner, L. Le Pleux, J. Petersson, Y. Pellegrin, E. Blart, L. Hammarström and F. Odobel, *J. Phys. Chem. C*, 2014, **118**, 103–113.
71 D. Ameline, S. Diring, Y. Farre, Y. Pellegrin, G. Naponiello, E. Blart, B. Charrier, D. Dini, D. Jacquemin and F. Odobel, *RSC Adv.*, 2015, **5**, 85530–85539.
72 G. A. Volpato, M. Marasi, T. Gobbato, F. Valentini, F. Sabuzi, V. Gagliardi, A. Bonetto, A. Marcomini, S. Berardi, V. Conte, M. Bonchio, S. Caramori, P. Galloni and A. Sartorel, *Chem. Commun.*, 2020, **56**, 2248–2251.
73 C. Decavoli, C. L. Boldrini, N. Manfredi and A. Abbotto, *Eur. J. Inorg. Chem.*, 2020, 978–999.

74 K. L. Materna, J. Jiang, K. P. Regan, C. A. Schmuttenmaer, R. H. Crabtree and G. W. Brudvig, *ChemSusChem*, 2017, **10**, 4526–4534.
75 J. Jiang, J. R. Swierk, K. L. Materna, S. Hedström, S. Hee Lee, R. H. Crabtree, C. A. Schmuttenmaer, V. S. Batista and G. W. Brudvig, *J. Phys. Chem. C*, 2016, **120**, 28971–28982.
76 J. R. Swierk, D. D. Méndez-Hernández, N. S. McCool, P. Liddell, Y. Terazono, I. Pahk, J. J. Tomlin, N. V. Oster, T. A. Moore, A. L. Moore, D. Gust and T. E. Mallouk, *Proc. Natl. Acad. Sci. U. S. A.*, 2015, **112**, 1681–1686.
77 J. T. Kirner, J. J. Stracke, B. A. Gregg and R. G. Finke, *ACS Appl. Mater. Interfaces*, 2014, **6**(16), 13367–13377.
78 J. T. Kirner and R. G. Finke, *ACS Appl. Mater. Interfaces*, 2017, **9**, 27625–27637.
79 M. Bonchio, Z. Syrgiannis, M. Burian, N. Marino, E. Pizzolato, K. Dirian, F. Rigodanza, G. A. Volpato, G. La Ganga, N. Demitri, S. Berardi, H. Amenitsch, D. M. Guldi, S. Caramori, C. A. Bignozzi, A. Sartorel and M. Prato, *Nat. Chem.*, 2019, **11**, 146–153.
80 F. Li, K. Fan, B. Xu, E. Gabrielsson, Q. Daniel, L. Li and L. Sun, *J. Am. Chem. Soc.*, 2015, **137**, 9153–9159.
81 D. Wang, M. S. Eberhart, M. V. Sheridan, K. Hu, B. D. Sherman, A. Nayak, Y. Wang, S. L. Marquard, C. J. Dares and T. J. Meyer, *Proc. Natl. Acad. Sci. U. S. A.*, 2018, **115**, 8523–8528.
82 Y. Zhu, G. Liu, R. Zhao, H. Gao, X. Li, L. Sun and F. Li, *Chem. Sci.*, 2022, **13**, 4955–4961.
83 N. Manfredi, C. L. Boldrini and A. Abbotto, *ChemElectroChem*, 2018, **5**, 2395–2402.
84 C. Decavoli, C. L. Boldrini, V. Trifiletti, S. Luong, O. Fenwick, N. Manfredi and A. Abbotto, *RSC Adv.*, 2021, **11**, 5311–5319.
85 T. G. Ulusoy Ghobadi, A. Ghobadi, M. Buyuktemiz, E. A. Yildiz, D. Berna Yildiz, H. G. Yaglioglu, Y. Dede, E. Ozbay and F. Karadas, *Angew. Chem.*, 2020, **132**, 4111–4119.
86 T. Luo, X. Li, C. Bai, C. Lv, J. Huang and J. Liu, *ACS Appl. Energy Mater.*, 2021, **4**, 14671–14680.
87 G. A. Volpato, E. Colusso, L. Paoloni, M. Forchetta, F. Sgarbossa, V. Cristino, M. Lunardon, S. Berardi, S. Caramori, S. Agnoli, F. Sabuzi, P. Umari, A. Martucci, P. Galloni and A. Sartorel, *Photochem. Photobiol. Sci.*, 2021, **20**, 1243–1255.
88 T. Li, H. Dong, Y. Hao, Y. Zhang, S. Chen, M. Xu and Y. Zhou, *Electroanalysis*, 2022, **34**, 956–965.
89 J. Shu and D. Tang, *Anal. Chem.*, 2020, **92**, 363–377.
90 Z. Wang, J. Li, W. Tu, H. Wang, Z. Wang and Z. Dai, *ACS Appl. Mater. Interfaces*, 2020, **12**, 26905–26913.
91 X. Yang, M. Zhang, Z. Chen, Y. Bu, X. Gao, Y. Sui and Y. Yu, *ACS Appl. Mater. Interfaces*, 2021, **13**, 16828–16836.
92 T. Shi, Z. Wen, L. Ding, Q. Liu, Y. Guo, C. Ding and K. Wang, *Sens. Actuators, B*, 2019, **299**, 126834–126842.
93 M. Li, S. An, Y. Wu, Z. Yan, Y. Chai and R. Yuan, *ACS Appl. Mater. Interfaces*, 2022, **14**, 53398–53404.
94 J. Hu, Z. Li, C. Zhai, L. Zeng and M. Zhu, *Anal. Chim. Acta*, 2021, **1183**, 338951–338960.
95 L. Huang, L. Yang, C. Zhu, H. Deng, G. Liu and Y. Yuan, *Sens. Actuators, B*, 2018, **274**, 458–463.
96 C. Zhao, L. Zhang, Q. Wang, L. Zhang, P. Zhu, J. Yu and Y. Zhang, *ACS Appl. Mater. Interfaces*, 2021, **13**, 20397–20404.
97 Y. Wang, Y. Cheng, N. Wu and Z. Zhang, *ACS Appl. Nano Mater.*, 2020, **3**, 8598–8603.
98 V. Mazzaracchio, R. Marrone, M. Forchetta, F. Sabuzi, P. Galloni, M. Wang, A. Nazligul, K. Choy, F. Arduini and D. Moscone, *Electrochim. Acta*, 2022, **426**, 140766–140774.
99 O. Suryani, Y. Higashino, J. Y. Mulyana, M. Kaneko, T. Hoshi, K. Shigakic and Y. Kubo, *Chem. Commun.*, 2017, **53**, 6784–6787.
100 D. Antón-García, J. Warnan and E. Reisner, *Chem. Sci.*, 2020, **11**, 12769–12776.
101 M. Forchetta, F. Sabuzi, L. Stella, V. Conte and P. Galloni, *J. Org. Chem.*, 2022, **87**, 14016–14025.
102 M. Forchetta, F. Valentini, V. Conte, P. Galloni and F. Sabuzi, *Catalysts*, 2023, **13**, 220–242.
103 H. Guo, H. Xia, X. Ma, K. Chen, C. Dang, J. Zhao and B. Dick, *ACS Omega*, 2020, **5**, 10586–10595.
104 W. Li, Z. Xie and X. Jing, *Catal. Commun.*, 2011, **16**, 94–97.
105 W. Li, L. Li, H. Xiao, R. Qi, Y. Huang, Z. Xie, X. Jing and H. Zhang, *RSC Adv.*, 2013, **3**, 13417–13421.
106 C. Ye, Y. Zhang, A. Ding, Y. Hu and H. Guo, *Sci. Rep.*, 2018, **8**, 2005.
107 B. Zhao, G. B. Hammond and B. Xu, *Tetrahedron Lett.*, 2021, **82**, 153776–153782.
108 B. Arnò, A. Coletta, C. Tesauro, L. Zuccaro, P. Fiorani, S. Lentini, P. Galloni, V. Conte, B. Floris and A. Desideri, *Biosci. Rep.*, 2013, **33**, 269–279.